

Thermal expansion of polymers: Mechanisms in orthorhombic polyethylene

J. A. O. Bruno,* N. L. Allan, T. H. K. Barron, and A. D. Turner
School of Chemistry, University of Bristol, Cantock's Close, Bristol, BS8 ITS, United Kingdom
 (Received 13 March 1998)

Quasiharmonic lattice dynamics is used to examine the mechanisms underlying the anisotropic thermal expansion of orthorhombic polyethylene, with particular attention to low temperature behavior. Several sets of interatomic potentials all give good qualitative agreement with experiment. Tensions caused by vibrations with components away from the bond directions are responsible for the negative expansion along the polymer chains, and contribute significantly to the expansion perpendicular to the chains; associated torques on the bonds have only a small effect, except at very low temperatures. The anisotropy of the expansion perpendicular to the chains results from a subtle interplay of thermal stress and elasticity. The results suggest that this anisotropy will be greatly reduced or even reversed at low temperatures. [S0163-1829(98)06437-6]

I. INTRODUCTION

In principle, the thermal expansion of simple solids is well understood.¹ It is driven predominantly by the effect of vibrations on central force interactions between neighboring atoms. Such models can account, for example, for the negative expansion observed at low temperatures in many tetrahedrally bonded crystals. Other crystals, however, show more complex behavior. This may be due to intricate electronic behavior, as in some magnetic and heavy fermion solids, but may also be due to the complexity of the crystal structure and bonding, and sometimes to disorder. Polymeric materials are a case in point, presenting formidable problems for the theorist, owing to their long chain structure and the consequent need for an accurate representation of the interplay of both the weak intermolecular and strong intramolecular forces. In addition, many polymeric materials are semicrystalline, making it difficult, if not impossible, to obtain reliable estimates of ideal crystalline behavior from experiment.

In the present paper we continue a systematic theoretical study of mechanisms underlying the thermal expansion of crystalline polymers, which has been under way in our group for some years. In this work the internal expansion (rearrangement of atoms within the unit cell) is treated simultaneously and on the same footing as the macroscopic expansion.^{1,2} After summarizing the conclusions reached from the study of skeletal chain models,³⁻⁵ we study several models and potentials for orthorhombic polyethylene (o-PE), with particular attention to the anisotropic thermal expansion at low and intermediate temperatures and the underlying mechanisms.

For this purpose it is efficient to use quasiharmonic lattice dynamics consistently in the first order approximation: the thermal expansion coefficients are calculated from analytic expressions, and evaluated at all temperatures for the geometry of the static lattice. This neglects all effects of higher order in the anharmonicity, including those due to the change of geometry with temperature. For a crystal as soft as polyethylene this would be a serious drawback for quantitative studies at most temperatures, but it is efficient for investigat-

ing mechanisms and is also quantitatively sound at sufficiently low temperatures.

We start in Sec. II by describing the crystal structure and the coordinates used to describe its state of strain, together with available experimental data on thermal expansion. Section III gives the background theory, including that of central force mechanisms of thermal expansion, together with a brief account of computational details of particular interest. Section IV summarizes earlier conclusions from skeletal chain models, before our present results for the expansion coefficients and Grüneisen functions of polyethylene are given in Sec. V. These include the contributions from different mechanisms, zero-point energy effects and behavior at low temperatures. Final remarks are in Sec. VI.

II. CRYSTAL STRUCTURE AND THERMAL EXPANSION

The orthorhombic unit cell is shown in Fig. 1. This primitive cell contains twelve atoms which belong to two conformationally-equivalent chains. The space group is *Pnam*.⁶ There are nine structural parameters: the lattice parameters a , b , and c , and six internal coordinates w_m ($m=1 \dots 6$) which determine the positions of all the atoms in frac-

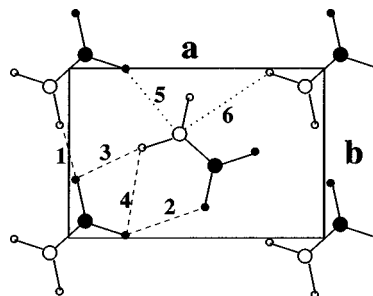


FIG. 1. Unit cell of ideal orthorhombic polyethylene. $a=7.121$ Å, $b=4.851$ Å, $c=2.548$ Å (Ref. 7). Atoms colored black are at height $\frac{1}{4}c$, empty circles denote a height of $-\frac{1}{4}c$. Large circles denote C atoms, small circles denote H atoms. Dashed lines show the H \cdots H intermolecular interactions considered, labelled by increasing distance: (1) 2.5349 Å, (2) 2.6330 Å, (3) 2.6597 Å, and (4) 2.8858 Å. Dotted lines show the C \cdots H interactions: (5) 3.1789 Å and (6) 3.3605 Å.

TABLE I. Arrangement of atoms in the unit cell of o-PE. $w_1 = 0.044183$, $w_2 = 0.059859$, $w_3 = 0.186360$, $w_4 = 0.011509$, $w_5 = 0.027079$, and $w_6 = 0.277646$.

Atoms	Fractional coordinates
C	$\pm(w_1, w_2, \frac{1}{4})$
H	$\pm(w_3, w_4, \frac{1}{4})$
H	$\pm(w_5, w_6, \frac{1}{4})$
C	$\pm(\frac{1}{2} - w_1, \frac{1}{2} + w_2, -\frac{1}{4})$
H	$\pm(\frac{1}{2} - w_3, \frac{1}{2} + w_4, -\frac{1}{4})$
H	$\pm(\frac{1}{2} - w_5, \frac{1}{2} + w_6, -\frac{1}{4})$

tional coordinates, as listed in Table I. We have taken the lattice parameters, measured at 4 K, from Ref. 7.

These nine parameters are convenient for the theory of internal expansion when developing algebraic expressions for use in computer codes, but for discussing the physical significance of the results we use equivalent sets with macroscopic strains $\eta_a = \delta \ln a$, $\eta_b = \delta \ln b$, $\eta_c = \delta \ln c$, and internal strains related directly to changes in distances between mean atomic positions and to changes in various angles determined by these positions, including the ‘‘setting angle’’ $\hat{\alpha}$ which the plane of a carbon chain makes with the ac -plane. Results obtained with different sets are related to each other by linear transformations.

The thermal expansion is highly anisotropic. The carbon chains run continuously in the c direction, and the coefficient of expansion α_c is negative. The expansion coefficients α_a and α_b perpendicular to the chains are positive, and larger than α_c by an order of magnitude or more. There is a less marked anisotropy in the ab -plane, with $\alpha_a > \alpha_b$ down to at least 100 K. At lower temperatures x-ray diffraction^{8,9} becomes insufficiently sensitive for expansion data (see Fig. 4 of Ref. 9). Much more precise dilatometric measurements can be made on bulk samples, with results extrapolated to 100% crystallinity.^{10,11} Isotropic material^{10,12} then gives a single coefficient α_{poly} . Drawn material¹² gives two, α_{\parallel} along the draw direction and α_{\perp} perpendicular to it; these are approximately equal to α_c and $(\alpha_a + \alpha_b)/2$, leaving undetermined the anisotropy in the ab plane at low temperatures. Accuracy obtainable by different experimental methods is reviewed in a recent handbook.¹³

III. THEORY

A. Quasiharmonic approximation

The effective potential energy Φ governing the lattice vibrations, as given for example by the Born-Oppenheimer approximation, is a function of the positions of the atoms, and can be expanded as a Taylor series in the displacements of the atoms from their mean positions:

$$\Phi = \Phi_0 + \Phi_1 + \Phi_2 + \Phi_3 + \Phi_4 + \dots, \quad (1)$$

where $\Phi_0 \equiv \Phi_{\text{stat}}$ is the static lattice energy and Φ_n denotes the term of order n in the displacements. In computations, the coefficients occurring in the Φ_n may be the input data defining a model, they may be derived from pair potentials or more general valence force-fields, or they may be obtained

from *ab initio* calculations. When a crystal structure has no internal degrees of freedom, the mean position of each atom is determined by symmetry and Φ_1 vanishes. When this is not so, a model in any state of internal strain can be maintained in equilibrium by applying appropriate internal stresses.

The harmonic approximation of lattice dynamics assumes that the amplitude of vibrations is sufficiently small for the anharmonic terms Φ_3 and beyond to be neglected. The vibrational motion is then a superposition of independent harmonic modes. In a periodic structure each mode is labelled by its wave vector \mathbf{q} and polarization s . For each wave vector the squares of the mode angular frequencies, $(\omega_{\mathbf{q}s})^2$, with their associated polarization vectors, are obtained as eigenvalues and eigenvectors of the Hermitian *dynamical matrix* $\mathbf{D}(\mathbf{q})$, which is derived in the usual way^{1,14} from the atomic masses and the coefficients occurring in the quadratic form Φ_2 .

The total Helmholtz free energy, F , is the sum of static and vibrational contributions:

$$F = \Phi_{\text{stat}} + F_{\text{vib}} \quad (2)$$

where the harmonic approximation gives F_{vib} as the sum of independent contributions from all the normal modes:

$$F_{\text{vib}} = \sum_{\mathbf{q}s} \left\{ \frac{1}{2} \hbar \omega_{\mathbf{q}s} + kT \ln \left[1 - \exp \left(- \frac{\hbar \omega_{\mathbf{q}s}}{kT} \right) \right] \right\}. \quad (3)$$

The *quasiharmonic approximation* obtains the strain-dependence of F_{vib} by applying the harmonic approximation afresh at each state of strain. The term ‘‘quasiharmonic’’ is used because for a truly harmonic crystal potential (with $\Phi_n = 0$ for $n > 2$) the coefficients in Φ_2 , and hence F_{vib} , would be independent of strain.¹ The approximation gives the thermal expansion coefficient correct to the first order in the anharmonicity of the potential (e.g., Ref. 15). In the present work, we keep consistently to this order of approximation, neglecting higher order effects; in particular we evaluate all quantities at the equilibrium geometry of the static lattice.¹⁶ Quantities are thus calculated as a function of temperature at constant strain, both internal and external. They should be close to constant pressure quantities at low temperatures, diverging at higher temperatures.

B. Thermodynamics of internal strain: the general regime

Through the frequencies, F_{vib} is a function both of external strain coordinates η_{λ} and of internal coordinates ϵ_k . Since crystal symmetry is preserved in thermal expansion, it is not necessary to consider all possible strains, but only a set of nine independent coordinates as described in Sec. II. In lattice dynamics it is convenient to treat all these strains simultaneously, as thermodynamic variables in the so-called ‘‘general regime.’’²

Together the η_{λ} and the ϵ_k comprise the set of generalized coordinates \mathcal{E}_A . The stresses \mathcal{T}_A thermodynamically conjugate to the \mathcal{E}_A are then

$$\mathcal{T}_A = \frac{1}{V} \left(\frac{\partial F}{\partial \mathcal{E}_A} \right)_{\epsilon', T}, \quad (4)$$

where $\overset{\circ}{V}$ is the volume of the reference configuration and so is independent of strain. The isothermal elastic stiffnesses follow by taking second order derivatives of F :

$$C_{\alpha\beta}^T = \left(\frac{\partial \mathcal{T}_A}{\partial \mathcal{E}_B} \right)_{\varepsilon', T} = \frac{1}{\overset{\circ}{V}} \left(\frac{\partial^2 F}{\partial \mathcal{E}_A \partial \mathcal{E}_B} \right)_{\varepsilon', T}. \quad (5)$$

The second order compliances

$$S_{AB}^T = \left(\frac{\partial \mathcal{E}_A}{\partial \mathcal{T}_B} \right)_{T', T} \quad (6)$$

are then found by inverting the entire stiffness matrix C_{AB}^T .

The heat capacity at constant macroscopic and internal strain is

$$C_\varepsilon = -T \left(\frac{\partial^2 F}{\partial T^2} \right)_\varepsilon \quad (7)$$

and the thermodynamic Grüneisen functions $\Gamma_A(T)$ are proportional to the thermal stress coefficients:

$$\Gamma_A(T) = -\frac{V}{C_\varepsilon} \left(\frac{\partial \mathcal{T}_A}{\partial T} \right)_\varepsilon. \quad (8)$$

The thermal expansion coefficients are given by

$$\mathcal{A}_A = -\sum_B S_{AB}^T \left(\frac{\partial \mathcal{T}_B}{\partial T} \right)_\varepsilon = \frac{C_\varepsilon}{V} \sum_B S_{AB}^T \Gamma_B(T). \quad (9)$$

They thus depend on the interplay of compliances and thermal stress coefficients, as discussed by Munn.¹⁷

Thermodynamically, Eqs. (4)–(9) are exact. But when the quasiharmonic approximation is used for F_{vib} and its derivatives, the vibrational contributions to the stresses \mathcal{T}_B and the consequent contributions to \mathcal{A}_A are correct only to the first order in the anharmonicity. Since the variation of elastic compliances with temperature is itself an anharmonic effect, we keep consistently to the lowest order in the anharmonicity by using the static lattice compliances in evaluating \mathcal{A}_A :

$$\mathcal{A}_A = \frac{1}{\overset{\circ}{V}} \sum_B S_{AB}^{\text{stat}} \sum_{\mathbf{q}s} \Gamma_B(\mathbf{q}, s) c \left(\frac{\hbar \omega_{\mathbf{q}s}}{kT} \right), \quad (10)$$

where $c(\hbar \omega/kT)$ is the heat capacity of a harmonic oscillator with frequency ω , and Γ_B is a mode Grüneisen parameter in this regime, defined by

$$\Gamma_B(\mathbf{q}, s) = - \left[\frac{\partial \ln \omega_{\mathbf{q}s}}{\partial \mathcal{E}_B} \right]_{\varepsilon'}. \quad (11)$$

In the computation, mode gammas are obtained from strain derivatives of the eigenvalues. These derivatives are obtained by first order perturbation theory.^{1,18,19}

C. Derivation of macroscopic properties

We use a different script to denote variables in the *macroscopic regime* of thermodynamics, which considers only external degrees of freedom η_λ , with conjugate stresses t_λ ,

expansion coefficients α_λ , stiffnesses $C_{\lambda\mu}$, etc. The definitions of these functions are analogous to those for the general regime; e.g.,

$$t_\lambda = \frac{1}{\overset{\circ}{V}} \left(\frac{\partial F}{\partial \eta_\lambda} \right)_{\eta', T}, \quad \alpha_\lambda = \left(\frac{\partial \eta_\lambda}{\partial T} \right)_t. \quad (12)$$

To relate macroscopic functions to those computed in the general regime, we remember that in macroscopic experiments the internal coordinates adjust to give minimum free energy, corresponding in the general regime to a condition of constant (zero) internal stress. We can therefore immediately identify the expansion coefficients \mathcal{A}_λ in the general regime with the macroscopic coefficients α_λ , since both correspond to conditions of constant internal and external stress. For the same reason, the macroscopic compliance matrix $S_{\lambda\mu}^T$ is the same as the submatrix $S_{\lambda\mu}^T$ of S_{AB}^T . In contrast, the stiffness submatrix $C_{\lambda\mu}^T$ does not give the macroscopic stiffnesses, because it refers to conditions of constant internal strain (rather than constant internal stress); instead, the $C_{\lambda\mu}^T$ are obtained by inverting the $S_{\lambda\mu}^T$ matrix. Similarly, the macroscopic Grüneisen functions, γ_λ , which are often used in the analysis of thermal expansion data, are defined by

$$\gamma_\lambda = -\frac{V}{C_\eta} \left(\frac{\partial t_\lambda}{\partial T} \right)_\eta. \quad (13)$$

The γ_λ allow for the relaxation of internal degrees of freedom, and so differ from the Γ_λ of the general regime.² To the present first order accuracy they are given by

$$\gamma_\lambda = \Gamma_\lambda - \sum_{k,m} \Gamma_k \mathfrak{G}_{km}^{\text{stat}} C_{m\lambda}^{\text{stat}}, \quad (14)$$

where $\mathfrak{G}_{km}^{\text{stat}}$ is the inverse of the internal submatrix C_{km}^{stat} of the matrix C_{AB}^{stat} . We also note in passing that the heat capacity given by the sum of harmonic mode contributions is not C_η but C_ε ; if required, it can be converted thermodynamically to the macroscopic properties C_η and C_p .^{1,2}

D. Integration grids

To evaluate thermodynamic properties, expressions involving the normal mode frequencies and their strain derivatives are integrated over the first Brillouin zone (FBZ). For o-PE the FBZ is rectangular, and symmetry enables us to restrict the numerical integration to the positive quadrant. Fine meshes were used to obtain high accuracy, and also to test the reliability of results from coarser meshes. For testing, two different types of meshes were employed, both obtained by dividing reciprocal space into cells similar in shape to the Brillouin zone but smaller in linear dimensions by a factor $1/m$. One mesh comprised the cell centers (the Monkhorst-Pack mesh²⁰); the other comprised the cell corners, except that the Γ point was omitted because it is a singular point for the Grüneisen parameters of acoustic modes.

For each mesh an iterative procedure was used to extend the accuracy of the integration to very low temperatures, where only low-frequency acoustic modes with \mathbf{q} vectors lying close to the Γ point contribute to the thermodynamic properties.^{5,19} In the first step the integration over the inner

TABLE II. Values of γ_b and γ_c for VFF2 at 1.0 K and at 100 K, obtained with varying mesh size in the FBZ for two different types of mesh. Faster convergence is obtained by combining them in accordance with Simpson's rule.

		γ_b					
		$T=1.0$ K			$T=100.0$ K		
Mesh	Center	Corner	Simpson's rule	Center	Corner	Simpson's rule	
4	3.080	3.109	3.090	1.229	1.489	1.316	
8	2.896	3.181	2.991	1.188	1.362	1.246	
16	2.850	3.060	2.920	1.215	1.275	1.235	
32	2.863	2.961	2.896	1.235	1.245	1.238	
48	2.883	2.926	2.897	1.239	1.241	1.240	
64	2.893	2.913	2.900	1.240	1.240	1.240	

		γ_c					
		$T=1.0$ K			$T=100.0$ K		
Mesh	Center	Corner	Simpson's rule	Center	Corner	Simpson's rule	
4	-20.34	-5.992	-15.56	-2.328	-1.601	-2.086	
8	-16.50	-11.87	-14.96	-1.603	-1.978	-1.728	
16	-15.71	-14.05	-15.16	-1.665	-1.793	-1.708	
32	-15.24	-14.84	-15.11	-1.707	-1.729	-1.714	
48	-15.10	-15.00	-15.07	-1.715	-1.720	-1.717	
64	-15.06	-15.04	-15.05	-1.717	-1.718	-1.717	

region with linear dimensions half that of the full zone is recalculated with a finer mesh employing the same number of points as that used originally for the full zone. In the next iteration the inner region of the first inner region is treated similarly, and so on until satisfactory convergence is obtained after three to six steps. The procedure had no significant effect on the results at temperatures above about 10 K, but was essential in the range down to 0.4 K, even for a mesh with $m=64$.

Convergence with increasing value of m proved slow for some of the quantities calculated, especially at low temperatures; and most of the final results were obtained from a Monkhorst-Pack mesh with $m=64$, giving a density of 262 144 points per zone (and much higher in the inner regions). Even so, for some quantities full convergence was not achieved, and for them a simple scheme based on Simpson's rule was applied. This will be described in more detail elsewhere.²¹ Examples of the degree of convergence achieved with different meshes are given in Table II for the macroscopic Grüneisen functions γ_b and γ_c .

E. Central force mechanisms for thermal stress

So far the theory given above applies to any type of crystal potential. This section considers specifically the action of pair potentials. The net thermal expansion of a crystal is its elastic response to the total thermal stress, and there are several ways in which thermal stresses arise in a central force model.

Bond-stretching effect. The most common intuitive explanation for thermal expansion is that atoms need more room in which to vibrate at higher temperatures. This crude oversimplification can be made more precise by considering the typical form of the interatomic potential (Fig. 2). The asymmetry of the form of the potential leads to an increase

of the mean interatomic distance with increasing amplitude of vibrations. An equivalent argument is to consider the mean interatomic distance held constant; as also illustrated in Fig. 2, the vibrations give rise to a time averaged force between the atoms which tends to increase the interatomic distance, and the thermal expansion is the elastic response to this force. This "bond-stretching" effect is dominant in the (positive) thermal expansion of many solids.

Tension effects. When the vibration includes components of relative motion perpendicular to the bond, the mean interatomic distance is greater than the distance between the mean atomic positions; the resulting increase in bond tension causes a thermal stress tending to contract the bond and so restore the mean interatomic distance to its equilibrium value (Fig. 3). When the relative motion also has a component along the bond, there is in addition a net torque tending to

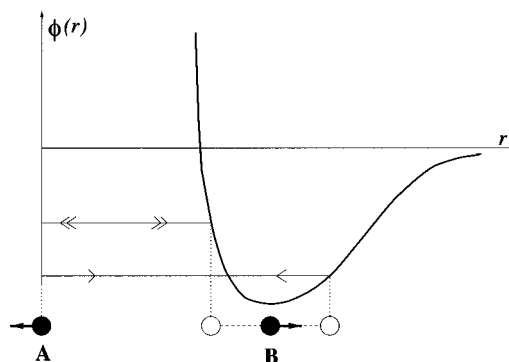


FIG. 2. Vibrational displacements along the internuclear direction between two atoms, which interact via an anharmonic pair potential, produce a mean repulsive force. Positions connected by the dashed line represent the amplitude of motion of atom B with respect to atom A.

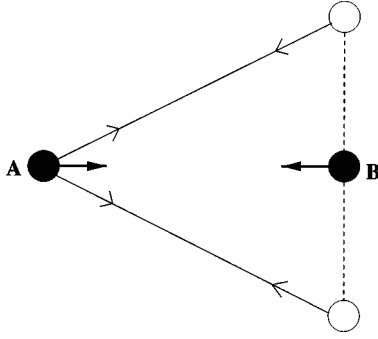


FIG. 3. Vibrational displacements perpendicular to the bond direction produce a mean attractive force. Positions connected by the dashed line represent the amplitude of motion of atom B with respect to atom A.

rotate the direction of the bond away from the direction of the relative motion²² (Fig. 4). Different vibrational modes tend to rotate the bond in different directions, and in cubic crystals the net effect is zero; but it is not zero for bonds in crystals of lower symmetry such as o-PE.

The contributions to each of these mechanisms to the strain derivatives of the dynamical matrix $\mathbf{D}(\mathbf{q})$ can be easily identified. Each potential $\phi(r)$ between two atoms separated by a vector \mathbf{r} contributes linearly to the elements of $\mathbf{D}(\mathbf{q})$, with terms proportional to the derivatives

$$\frac{\partial^2 \phi}{\partial r_\alpha \partial r_\beta} = \left(\phi'' - \frac{\phi'}{r} \right) c_\alpha c_\beta + \frac{\phi'}{r} \delta_{\alpha\beta}, \quad (15)$$

where $c_\alpha = r_\alpha/r$ and $c_\beta = r_\beta/r$ are the direction cosines of the bond. When the crystal is subject to a perturbing strain, \mathbf{r} may change in both length and direction:

$$r \rightarrow r + \Delta r, \quad c_\alpha c_\beta \rightarrow c_\alpha c_\beta + \Delta(c_\alpha c_\beta).$$

The consequent perturbation in $\mathbf{D}(\mathbf{q})$ thus contains a contribution proportional to

$$\Delta \left(\frac{\partial^2 \phi}{\partial r_\alpha \partial r_\beta} \right) = (\Delta \phi'') c_\alpha c_\beta + \Delta \left(\frac{\phi'}{r} \right) (\delta_{\alpha\beta} - c_\alpha c_\beta) + \left(\phi'' - \frac{\phi'}{r} \right) \Delta(c_\alpha c_\beta), \quad (16)$$

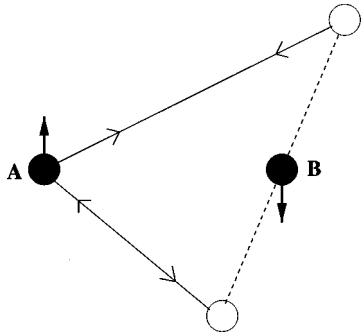


FIG. 4. Vibrational displacements with components both along and perpendicular to the bond direction produce a mean torque on the bond in addition to the forces shown in Figs. 2 and 3. Positions connected by the dashed line represent the amplitude of motion of atom B with respect to atom A.

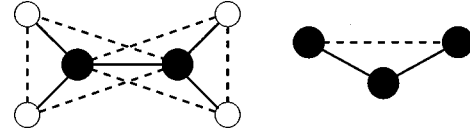


FIG. 5. Three types of "struts" (C - - C, C - - H, H - - H) between next-nearest neighbors used to simulate three-body angle forces. Filled circles: C atoms; empty circles: H atoms.

where the terms on the right-hand side (RHS) are due respectively to changes in the pair force constant, in the tension, and in the bond direction. The corresponding terms in the third order derivatives occurring in the perturbation matrix $\mathbf{D}'(\mathbf{q})$ are

$$\begin{aligned} \frac{\partial}{\partial r_\gamma} \left(\frac{\partial^2 \phi}{\partial r_\alpha \partial r_\beta} \right) &= (r \phi''') \frac{r_\alpha r_\beta r_\gamma}{r^4} + \left(\phi'' - \frac{\phi'}{r} \right) \\ &\times \left(r_\gamma \delta_{\alpha\beta} - \frac{r_\alpha r_\beta r_\gamma}{r^2} \right) + \left(\phi'' - \frac{\phi'}{r} \right) \\ &\times \left(r_\alpha \delta_{\beta\gamma} + r_\beta \delta_{\alpha\gamma} - \frac{2r_\alpha r_\beta r_\gamma}{r^2} \right), \quad (17) \end{aligned}$$

where the terms on the RHS are, respectively, the bond stretching, nonrotational tension, and rotational tension contributions. We can therefore readily study the relative importance of the different effects.

F. Analysis of internal adjustments within the unit cell

In some crystal structures the readjustment of atomic positions within the unit cell has a major effect on the macroscopic thermal expansion. A striking example is provided by α quartz, where the ability of the SiO_4 tetrahedra to rotate easily gives rise to positive thermal expansion, whereas for other silica structures without this ability the expansion is negative.

With an appropriate choice of internal strain coordinates the present analysis permits the study of such effects; not only does it reveal how the coordinates change with temperature, but also by constraining one or more of them to remain constant we can study the effect of their relaxation on the temperature dependence of other strains. Theoretically, such "clamping" reduces the number of active strains and stresses, \mathcal{E}_A and \mathcal{T}_A , but does not change the values of the thermal stress coefficients, Grüneisen functions and elastic stiffnesses \mathcal{C}_{AB} for those that remain. The new compliances \mathcal{S}_{AB} are obtained by inverting the matrix \mathcal{C}_{AB} for the clamped crystal, which is simply a submatrix of that for the unclamped crystal; and the remaining properties follow as described earlier.

IV. CONCLUSIONS FROM SKELETAL CHAIN MODELS

We summarize here conclusions reached previously in this laboratory from studying a series of central-force skeletal chain models of increasing complexity.³⁻⁵ Properties of the models were evaluated at a fixed geometry (static equilibrium). Short-range pair potentials $\phi(r)$ were used, with

TABLE III. Parameter listings. For intramolecular pair potentials, including struts, $r\phi'''/\phi''$ was set to -21 (the value given by a 6-12 potential when $\phi'=0$), except that for VFF2 they came from the Morse potential in GULP (Ref. 26) and for VFF4 $\phi_s'''=0.25\phi_s'''^{VFF2}$. All intramolecular potentials were fitted to a Buckingham form, except for VFF4 where $\phi'''[\text{H}\cdots\text{H}$ (3) and (4)]= $1.25\phi'''^{VFF2}$ and both $\phi'''[\text{C}\cdots\text{H}] = 0.50\phi'''^{VFF2}$. For all interactions ϕ' was put equal to zero.

Type		Strut model force-fields (N m^{-1})				
		BRC	BT	VFF1	VFF2	VFF4
C—C bond:	ϕ''	400.00	400.00	220.704	208.155	208.155
	ϕ'''	-8400.00	-8400.00	-4634.784	-3193.816	-3193.816
C—H bond:	ϕ''	400.00	400.00	220.704	208.055	208.055
	ϕ'''	-8400.00	-8400.00	-4634.784	-2260.558	-2260.558
C - -C strut:	ϕ''	100.00	100.00	150.425	102.379	102.379
	ϕ'''	-2100.00	-2100.00	-3158.925	-2149.959	-537.490
C - -H strut:	ϕ''	100.00	100.00	127.813	103.577	103.577
	ϕ'''	-2100.00	-2100.00	-2684.073	-2175.117	-543.779
H - -H strut:	ϕ''	100.00	100.00	126.342	101.243	101.243
	ϕ'''	-2100.00	-2100.00	-2653.182	-2126.103	-531.526
H \cdots H (1): ^a	ϕ''	1.000	0.413	0.413	0.484	0.484
	ϕ'''	-21.000	-5.264	-5.264	-5.595	-5.595
H \cdots H (2): ^a	ϕ''	1.000	0.432	0.432	0.509	0.509
	ϕ'''	-21.000	-5.476	-5.476	-5.832	-5.832
H \cdots H (3): ^a	ϕ''	1.000	0.201	0.201	0.212	0.212
	ϕ'''	-21.000	-2.834	-2.834	-2.864	-3.580
H \cdots H (4): ^a	ϕ''	1.000	0.806	0.806	1.008	1.008
	ϕ'''	-21.000	-9.373	-9.373	-10.305	-12.884
C \cdots H (5): ^a	ϕ''		0.273	0.273	0.291	0.291
	ϕ'''		-5.410	-5.410	-4.301	-2.151
C \cdots H (6): ^a	ϕ''		0.122	0.122	0.142	0.142
	ϕ'''		-2.974	-2.974	-2.428	-1.214
Torsion CCCC: ^b	τ		4.700	4.700	4.700	4.700

^aLabeling as in Fig. 1.

^bFrom Ref. 24, by Eq. (19).

$\phi'=0$ and $r\phi''' = -21\phi''$ as at the minimum of the 6-12 potential

$$\phi(r) = \epsilon_0 \{-2(r/r_0)^6 + (r/r_0)^{12}\}. \quad (18)$$

Thus ϕ'' was the variable parameter specifying the interaction between a pair of atoms. Intramolecular potentials were taken between successive atoms in the chains (bond: ϕ_b), and between next-nearest successive atoms in zigzag chains (strut: ϕ_s). A much weaker potential was taken between nearest neighbors in adjacent chains (interchain: ϕ_i), and most of the models were constructed so that all interacting pairs of atoms in different chains were at the same distance apart. The axis Oz was taken along the chain direction, and for crystals of parallel zigzag chains Oy was perpendicular to the molecular plane. The models had orthorhombic, tetragonal or trigonal symmetry. All of the cross-compliances S_{23} , S_{13} , S_{12} were negative, giving positive Poisson's ratios.

The first models studied consist of parallel linear chains. They are easily compressible in the xy plane, with S_{11} , S_{22} , S_{12} large, and incompressible along Oz , with S_{33} , S_{13} , S_{23} very small. Vibrations polarized along the chain lengths are mostly of high frequency, of small amplitude and not excited at low and intermediate temperatures. The amplitude of the excited atomic vibrations is therefore mainly perpendicular

to the chains, so that the thermal expansion in the chain direction is dominated by tension effects and is small and negative. In contrast, the much weaker interchain interactions give rise both to positive bond stretching and to negative tension effects, which depend on the angles made with the polarization directions for each vibrational mode. Both effects are appreciable, but the bond-stretching effect is greater, resulting in a large approximately isotropic expansion perpendicular to the chains.

Crystals of parallel planar zigzag chains behave differently. In the absence of struts ($\phi_s=0$) the chains are flexible, and stress along the chain can be largely relaxed by changing the CCC angle, affecting both the elasticity and the thermal stress; the crystals are no longer incompressible along Oz , and the final macroscopic thermal stress is no longer strongly anisotropic. Results depend on details of the geometry. For a chain angle of 90° the thermal stress is almost isotropic, and $S_{11}=S_{22}=S_{33}$; but a very strongly negative cross-compliance S_{13} in the plane of the molecular chains lowers the expansion in directions Ox and Oz parallel to the molecular planes below that in the perpendicular direction Oy . For a different geometry with a tetrahedral chain angle, there is greater anisotropy in both thermal stress and elasticity; the expansion coefficients are still all positive, with α_y greatest; but α_z is now much smaller than α_x .

When the chains are stiffened by struts between second neighbors, stresses along the chain direction can no longer be relaxed easily by internal rearrangement. Negative expansion along the chain direction is restored, and S_{13} is small again. Thermal expansion remains greatest in the direction perpendicular to the molecular chains except at very low temperatures.

The final skeletal models examined approach more closely the geometry of polyethylene. All chains run in the same direction Oz , but the molecular planes are no longer all parallel but made alternately angles $\hat{\alpha}$ and $-\hat{\alpha}$ to the Oxz plane. For all these models the expansion is small and negative along the chain direction and large and positive in perpendicular directions, but the anisotropy in the Oxy plane is model dependent. A geometry based roughly on polyethylene, with $\hat{\alpha}=42^\circ$ and a tetrahedral bond angle, gives a moderate anisotropy with $\alpha_b > \alpha_a$ (opposite to that observed experimentally); but with a bond angle of 90° the expansion in the Oxy plane is virtually isotropic.

Thus for all the skeletal models the tension effect, due primarily to vibrations perpendicular to the polymer planes, is responsible for negative expansion in the chain direction; but expansion perpendicular to the chains is due to a combination of both bond stretching and tension effects, and its anisotropy is strongly model dependent. We shall see that this remains true for models of polyethylene, although the addition of H atoms changes the detailed behavior, including the nature of the anisotropy in the ab plane.

V. MODELS FOR POLYETHYLENE

The models used here for polyethylene are developed from those described above for skeletal polymers. Intramolecular pair potentials are now required for C—H bonds in addition to the C—C bonds, and for C—H and H—H ‘struts’ in addition to the C—C struts, so as to stiffen the all the tetrahedral angles at each carbon (Fig. 5). Intermolecular pair potentials are taken between all pairs of hydrogen atoms $H \cdots H$ less than 3 \AA apart, and for most of the models also between carbon and hydrogen atoms $C \cdots H$ less than 4 \AA apart. Most of the models include a harmonic intramolecular torsional potential for each sequence of four carbon atoms in the chains, of the form $\tau(h_1 - h_2 - h_3 + h_4)^2/2$, where h_n is the displacement of atom n normal to the skeletal plane.

Because we are using the first order approximation of evaluating the thermal expansion coefficients for the geometry of the static lattice, the pair potentials of the models are completely specified by giving the values of ϕ' , ϕ'' , and ϕ''' for each pair of interacting atoms (Table III), together with that of the torsional constant τ . We shall give the reasons for the choice of these models, by explaining their relation to others in the literature.

We start with the simplified model described in Ref. 5, which has no $C \cdots H$ interactions and has the same force-constants for all $H \cdots H$ pairs less than 3 \AA apart. It has also no torsional force constants, so that restoring forces for torsional oscillations are due solely to the $H \cdots H$ interactions. Rounded values are taken for the ϕ'' , based on published valence force fields, and again $r\phi''' = -21\phi''$. Unfortunately, the results for the expansion coefficients in Ref. 5

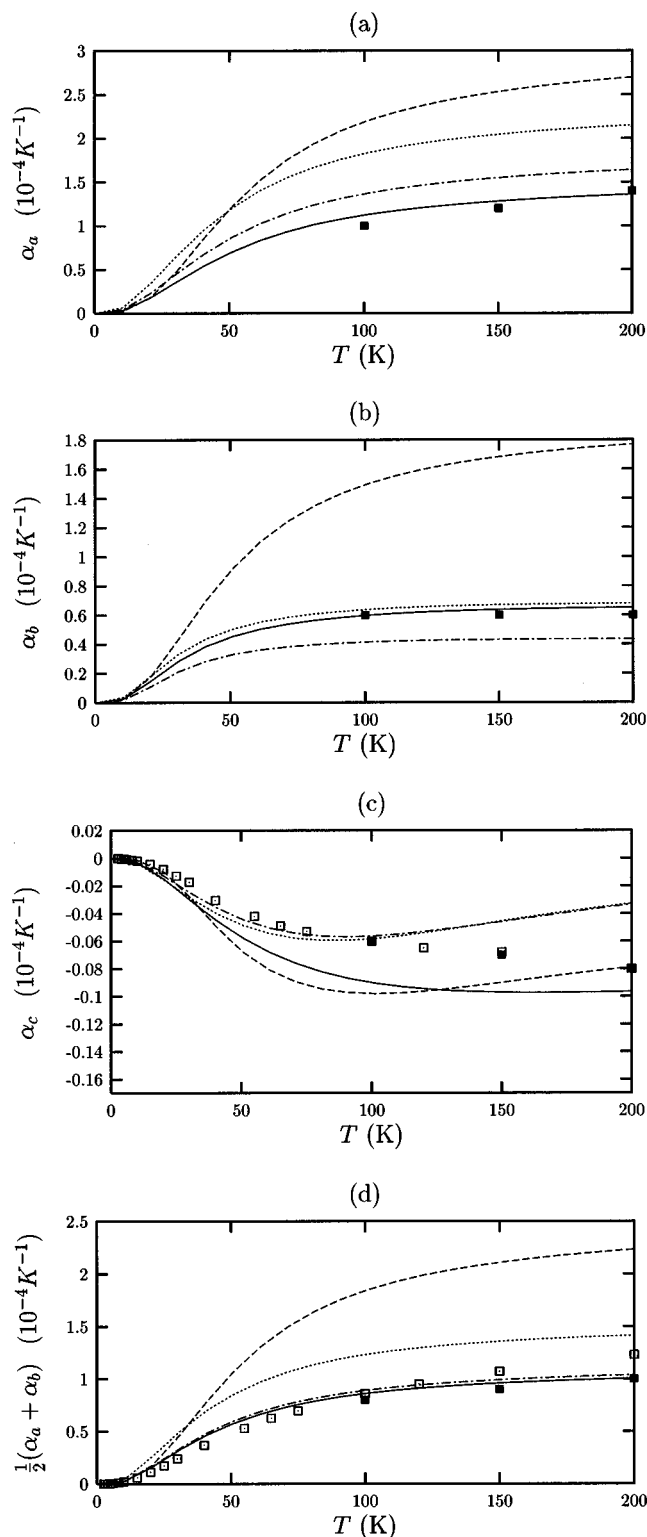


FIG. 6. Macroscopic thermal expansion as a function of temperature. —, BRC; ···, BT; - - -, VFF2; —, VFF4. Expt.: ■, Ref. 9; □, Ref. 12.

were incorrect, due to a small programming error. Corrected results for this model (hereafter referred to as model BRC) give much poorer quantitative agreement with experiment (see Fig. 6) than reported in Ref. 5, although the qualitative agreement with experiment remains encouraging, including the anisotropy perpendicular to the chains.

We therefore make a number of simultaneous refinements

TABLE IV. Calculated elastic stiffnesses (GPa).

	BRC	BT	VFF1	VFF2 / VFF4	Ref. 28	Ref. 30	Expt.
C_{11}	12.32	6.35	6.34	7.33	12.6	7.99	11.5 ^a
C_{12}	6.18	3.44	3.43	3.92	6.5	3.28	
C_{13}	4.09	2.21	2.06	2.39	2.1	1.13	
C_{22}	12.72	8.24	8.24	9.89	12.4	9.92	
C_{23}	5.28	3.42	3.20	3.85	4.3	2.14	
C_{33}	312	312	456	313	316	316	290 ^b
C_{44}	4.88	3.11	3.12	3.76		3.19	
C_{55}	4.74	2.08	2.08	2.33		1.62	
C_{66}	5.93	3.28	3.29	3.77		3.62	

^aAt 77 K, from Ref. 30.

^bFrom Ref. 31.

to the model: the 3 Å cutoff is retained for the H···H interactions, but they become a function of distance; and both C···H interactions (with a cutoff of 4 Å) and the torsional potential are added. For simplicity we retain the zero values for ϕ' for all pair interactions, but the value of $r\phi'''/\phi''$ varies.

We have investigated extensively the parametrization of the pair potentials in a series of models. For intramolecular potentials, in addition to using the parameters of BRC (in model BT), we have tested parameters derived from the Urey-Bradley force field of Tashiro *et al.*²³ (in model UBFF) and from three different valence force fields: one taken from Kobayashi and Tadokoro²⁴ (in model VFF1); one developed by us during this work (in model VFF2); and one taken from Hwang *et al.*²⁵ (in model VFF3). We have converted the force field parameters into force constants appropriate for our strut model, but it is important to note that this translation is not exact. Valence force fields have a greater number of second order force constants than the strut models, and so struts cannot reproduce all the features of a valence force field; while struts are fully adequate for keeping an angle rigid, they are not wholly satisfactory for describing properties which depend on departures from rigidity. The torsional force-constant τ was obtained from the parameter g_τ of Kobayashi and Tadokoro²⁴ by the transformation

$$\tau = g_\tau / (R \sin \theta)^2, \quad (19)$$

where R is the C—C distance and θ is the C—C—C angle.

For intermolecular potentials the same set of Buckingham potentials, of the form

$$\phi(r) = A \exp(-r/\rho) - C/r^6 \quad (20)$$

was taken from Ref. 24 and used to derive ϕ'' and ϕ''' values for models BT, UBFF, VFF1, and VFF3; for VFF2 the potentials were determined by using the program GULP,²⁶ with the criterion that the calculated equilibrium structure in the static limit reproduced closely the experimental structure. None of the models includes long-range Coulombic interactions — unlike, for example, that of Karasawa *et al.*²⁷ Of our models, BT, VFF1, VFF2, and a later modification VFF4 (see below) give the most satisfactory general agreement with experiment. It is for these, together with BRC, that we present results here; their potential parameters are listed in Table III.

Because elasticity plays an important role in thermal expansion, we list in Table IV the elastic stiffnesses in the static limit for the five models. It is clear that they are in general comparable to those of previous work.

A. Zero-point dilation and macroscopic expansion coefficients

To estimate the zero-point dilation at $T=0$ from static lattice equilibrium geometry, we retain only the first term on the RHS in Eq. (3). Each mode contributes $(\hbar\omega/2)$ to the zero-point energy, and so high frequency modes are important here; whereas only low frequency modes are thermally excited at low temperatures and so determine the subsequent expansion as the temperature is raised above $T=0$. Table V gives macroscopic dilations at $T=0$ along the a , b , and c axes for models BT, VFF1, VFF2, and VFF4, as calculated from $(\hbar/2V)\sum_B S_{AB}^T \sum_{q_s} \Gamma_B(\mathbf{q}, s) \omega_{q_s}$. All the dilations are positive and bond-stretching modes dominate. The magnitude of the dilations in the a , b , and c directions are given in Table V; VFF4 is closest to the estimates of Lacks and Rutledge.²⁸

The macroscopic expansion coefficients computed for the BRC, BT, VFF2, and VFF4 potentials are compared with experiment in Fig. 6 and for all five models at selected temperatures in Table VI; also, α_{\parallel} and α_{\perp} derived from measurements on drawn samples are compared with α_c and $(\alpha_a + \alpha_b)/2$ in Figs. 6(c) and 6(d). Each model has the same qualitative agreement with experiment as obtained previously,⁵ including the correct sign of the anisotropy in the ab plane.

The BT model gives better agreement with experiment than the BRC model, in two ways. First, there is much closer agreement with experiment for α_c between 40 and 100 K, which is low enough for the lowest order quasiharmonic ap-

TABLE V. Macroscopic dilations (%) due to the inclusion of zero-point effects.

Strain	Force fields				Ref. 28
	BT	VFF1	VFF2	VFF4	
η_a	4.15	4.19	3.52	2.48	1.93
η_b	2.91	3.07	2.50	1.78	1.48
η_c	0.31	0.40	0.20	0.12	0.47

TABLE VI. Macroscopic expansion coefficients (10^{-6} K^{-1}) given by different force fields.

	T (K)	Force fields					Experiment		
		BRC	BT	VFF1	VFF2	VFF4	Ref. 8	Ref. 9	Ref. 12
α_a	1	0.00185	0.00681	0.00679	0.00418	0.00320			
	10	1.89	5.95	5.50	3.56	2.79			
	20	16.18	31.71	30.49	21.09	16.50			
	40	83.46	93.74	91.07	66.40	53.02	0.5×10^2		
	100	218.9	182.6	179.2	136.6	112.4	1.0×10^2	1.0×10^2	
	150	253.3	204.6	201.2	155.0	128.2	1.3×10^2	1.2×10^2	
	200	269.7	215.0	211.7	164.2	136.1	1.5×10^2	1.4×10^2	
α_b	1	0.00268	0.00440	0.00428	0.00230	0.00307			
	10	2.34	3.20	2.94	1.73	2.40			
	20	16.52	17.25	16.32	10.36	13.94			
	40	67.40	42.85	41.11	27.83	37.72			
	100	149.2	63.65	61.90	41.38	59.68	0.5×10^2	0.6×10^2	
	150	168.4	66.88	65.63	43.11	63.70	0.61×10^2	0.6×10^2	
	200	176.9	67.90	67.07	43.51	65.07	0.63×10^2	0.6×10^2	
α_c	1	-0.00020	-0.00096	-0.00094	-0.00066	-0.00067			
	10	-0.13	-0.37	-0.34	-0.28	-0.31			-0.175
	20	-0.93	-1.51	-1.47	-1.25	-1.45			-0.79
	40	-4.88	-3.95	-4.17	-3.52	-4.43			-3.05
	100	-9.80	-5.83	-7.66	-5.63	-9.01	-0.1×10^2	-6	-6.0
	150	-9.00	-4.55	-7.57	-4.59	-9.71	-0.1×10^2	-7	-6.8
	200	-7.89	-3.28	-6.88	-3.33	-9.65	-0.1×10^2	-8	-8.0

proximation to be fair. Secondly, the magnitudes of α_a and α_b are considerably smaller than for BRC.

VFF1 gives only a slight improvement on the results for BT, but VFF2 is distinctly better for both α_c and $(\alpha_a + \alpha_b)/2$. However, all the first four sets predict incorrectly that α_c should decrease in magnitude above 100 K. This is due to the excitation of longitudinal compressive modes along the chains, which contributes positively to α_c because of the asymmetric C- -C strut. The disagreement with experiment may of course be due to the neglect of higher order anharmonic effects, but it suggests that a strut with the anharmonicity of a typical interatomic potential overestimates the anharmonicity of the valence bond angle.

We therefore developed model VFF4, which has the same harmonic force constants as VFF2 but has much less anharmonicity in the struts (see Table III); in addition, adjustments have been made to the anharmonic parameters of some of the intermolecular interactions so as to give closer agreement with the experimental anisotropy in the ab plane. As expected, this removes the marked rise in α_c above 100 K; but agreement is now poorer at low temperatures.

B. Mechanisms

The calculations reveal explicitly the separate contributions from the tension mechanisms (Sec. III). The BT, VFF1, VFF2, and VFF4 models all lead to the same general conclusions. For α_a , the *negative* nonrotational tension effects are approximately in the range 10–25 % of the *net* positive values. The rotational tension contribution is appreciable only at low temperatures, ranging from $\sim 10\%$ of the *net* positive values below 10 K to $< 1\%$ at 150 K. For α_b the nonrotational tension effect is relatively large, varying be-

tween 40 to 90% of the *net* positive value for BT, VFF1 and VFF4, or 55 to 130% for VFF2. The rotational contribution ranges from $\sim 15\%$ below 10 K to $\sim 3\%$ at 150 K for all models. The net positive thermal expansion in the ab plane is due to the dominant bond-stretching effect, but the large contributions of the tension effects are important in any quantitative study. In particular, at low temperatures the rotational contributions to α_a and α_b are of opposite sign, reducing α_a and increasing α_b , thus having a marked effect on the anisotropy in the ab plane.

Conversely, there are large positive bond-stretching contributions to α_c , which in magnitude range from 60% (VFF1) up to 160% (BT and VFF2) of the *net* negative values at 150 K. We confirmed that this is due chiefly to the anharmonicity of the C- -C strut pair potential by examining the effect of putting $\phi''' = 0$ in Eq. (17) for each strut potential in turn; when ϕ''' was set to zero for the C- -C strut, the calculated values of α_c no longer passed through a minimum with increasing temperature. In VFF4, which has a low value of ϕ''' for the C- -C strut, the bond-stretching contribution to α_c is only 4% at 150 K. The rotational tension contribution to α_c is negligible at low temperatures, but above 100 K is of the order of 10% of the nonrotational contribution, with opposite sign.

C. Internal expansion

Consider first the configuration of the individual molecular chains. The increasing amplitude of vibrations perpendicular to the C—C bonds leads to a decrease in the distance R between the mean positions of the carbon atoms, while leaving the instantaneous C—C bond distances virtually unchanged. The proportional decrease in R is larger than that of

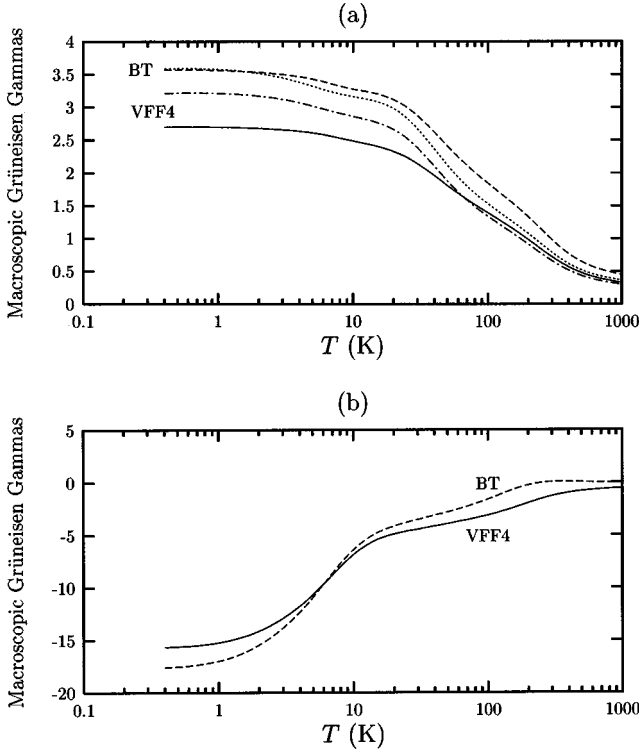


FIG. 7. Macroscopic Grüneisen parameters as a function of temperature. (a) γ_a : --, BT; —, VFF4. γ_b : ···, BT; -·-·, VFF4. (b) γ_c : --, BT; —, VFF4.

the c lattice parameter; this is as expected since, neglecting correlation between the motions of the atoms, we are considering the same amplitude of vibration perpendicular to the carbon chain and R is smaller than c .

Because of this the contractions in R and c lead to an increase of the apparent C—C—C angle with temperature, and a decrease in the width of the skeletal polymer ribbon. Calculations altering in turn the anharmonicity of the intramolecular C—C bonds and C—C struts confirm that the former produces a larger change in α_R than in α_c , while the latter has the opposite effect. For the C—H bonds too, the tension nonrotational effect is predominant, leading to a contraction of the distance between the mean C and H positions. Several interactions are responsible for the overall change in the H—C—H angle, which decreases with temperature.

The setting angle $\hat{\alpha}$ determines the relative orientation of neighboring chains, and its variation with temperature can be expected to affect the nature of the expansion perpendicular to the chain direction. For all our models $\hat{\alpha}$ decreases with temperature over the whole range; for VFF2 the change between 0 and 300 K is about 0.5° . The effect of this molecular rotation on the macroscopic expansion at 100 K is to diminish α_a by about 2.5% and to enhance α_b by about 6%.

D. Grüneisen functions and parameters

Examples of the calculated temperature variation of the macroscopic Grüneisen functions γ_λ defined in Eq. (13) are given in Fig. 7. For all our models γ_a and γ_b are both positive and decrease with temperature; γ_c is large and negative at low temperatures, becoming much smaller at high temperatures. By the macroscopic analog of Eq. (9), the expansion coefficients α_λ are related to the γ_λ through the compliances $S_{\lambda\mu}$:

$$\alpha_\lambda = \frac{C_\eta}{V} \sum_{\mu=1}^3 S_{\lambda\mu}^T \gamma_\mu. \quad (21)$$

When γ_a and γ_b are approximately equal, the anisotropy $\alpha_a > \alpha_b$ arises because $S_{11} > S_{22}$ (see Table VII). However, the negative cross-compliance S_{12} causes γ_b to contribute negatively to α_a and γ_a similarly to α_b , and a comparatively small change with temperature in the anisotropy of thermal stress in the ab plane brings about a much greater change in the anisotropy of expansion; thus for VFF4 the expansion is almost isotropic as $T \rightarrow 0$, where $\gamma_a/\gamma_b = 0.84$. In contrast, all contributions to α_c are negative; in VFF2 γ_a and γ_b together contribute 27% to α_c at 100 K.

E. Expansion at very low temperatures

As the temperature is lowered the contribution of higher frequency modes to the thermodynamic properties is progressively diminished, until finally the Debye elastic limit is reached. A close approach to the Debye limit is observed only at very low temperatures. It can be analyzed by plotting α_λ/T^3 and γ_λ against T^2 , and extrapolating to $T=0$. Even at 1 K there are appreciable differences from Debye values; e.g., for VFF2, α_a differs by 1%, α_b by 2% and α_c by 4%.

We have already seen that the ratio α_a/α_b decreases with temperature. To illustrate what happens at the lowest temperatures, we scale the expansion coefficients by the temperature-dependent Brugger factor²⁹ $\chi C_\epsilon/V$ to obtain dimensionless quantities of order unity. The most striking change is observed for BRC, where the anisotropy in the ab plane is reversed below 20 K (Fig. 8); but for all the models the ratio α_a/α_b as $T \rightarrow 0$ falls to roughly half of its 100 K value. Since the experimental value of this ratio at 100 K is about 2, this suggests that at low temperatures the expansion of o-PE in the ab plane is almost isotropic, as predicted by VFF4.

The values of α_c at very low temperatures depend almost entirely on the torsional oscillations of the carbon chain, by means of the nonrotational tension mechanism. For all models except BRC their magnitudes are well above the experimental α_\parallel (Table VI); the models thus overestimate the amplitude of these vibrations, indicating that the combined torsional and intermolecular potentials do not stiffen the

TABLE VII. Calculated elastic compliances $S_{\lambda\mu}$, $\lambda=1 \dots 3$, $\mu=1 \dots 3$ (10^{-2} GPa $^{-1}$).

	BRC			BT			VFF2/VFF4		
10.74	-5.199	-0.053	20.36	-8.470	-0.052	17.32	-6.847	-0.048	
-5.199	10.44	-0.108	-8.470	15.71	-0.112	-6.847	12.86	-0.106	
-0.053	-0.108	0.323	-0.052	-0.112	0.323	-0.048	-0.106	0.321	

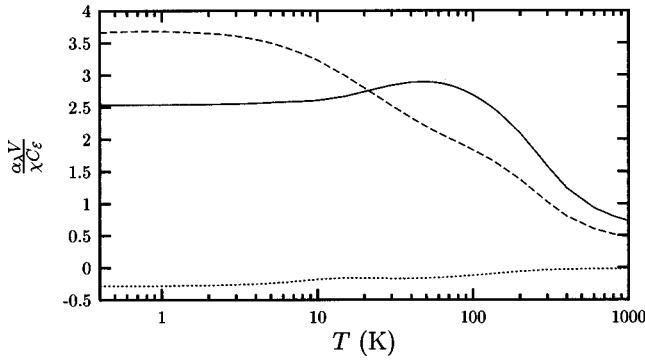


FIG. 8. The variation of $\alpha_\lambda V / \chi C_\epsilon$ with temperature for the BRC model. —, α_a ; --, α_b ; ···, α_c .

chain sufficiently. Since these vibrations also are important for expansion in the ab plane, this too will be overestimated at low temperatures.

F. Polycrystalline behavior

An isotropic bulk crystalline polymer, with Grüneisen function γ_{poly} , consists of randomly oriented crystallites. If the thermal expansion of a single crystal is anisotropic, the strain and stress fields within a polycrystalline sample are not uniform, but depend on the morphology; and so the expansion coefficient of the sample cannot be calculated exactly from the single crystal properties. There are however two classical approximations, due to Reuss and Voigt, which give upper and lower bounds for polycrystalline properties.³² In the Reuss approximation, the isotropic stress of the bulk is assumed to be uniform throughout the polycrystal, as in a fluid. For orthorhombic symmetry this leads to a coefficient of linear expansion

$$\alpha_{\text{poly}} \approx \frac{1}{3}(\alpha_a + \alpha_b + \alpha_c) = \alpha_{\text{Reuss}} \quad (22)$$

and a Grüneisen function

$$\gamma_{\text{poly}} \approx \frac{\gamma_a \chi_a^S + \gamma_b \chi_b^S + \gamma_c \chi_c^S}{\chi_a^S + \chi_b^S + \chi_c^S} = \gamma_{\text{Reuss}}, \quad (23)$$

where the χ_λ are linear compressibilities: $\chi_\lambda = \sum_{\mu=1}^3 S_{\lambda\mu}$. Thus the Reuss approximation gives γ_{poly} as an average of γ_a , γ_b , and γ_c weighted by the corresponding adiabatic linear compressibilities, and α_{poly} as one third of the volumetric expansion coefficient of a single crystal.

In the Voigt approximation it is the strain that is assumed to be uniform throughout the polycrystal, so that any isotropic volume change in the bulk produces an isotropic volume change in each crystallite. This leads to a thermal expansion coefficient which is an average of $\alpha_a, \alpha_b, \alpha_c$ weighted by $(C_{11}^T + C_{12}^T + C_{13}^T)$, etc., and a Grüneisen function that is an arithmetic average:

$$\gamma_{\text{poly}} \approx \frac{1}{3}(\gamma_a + \gamma_b + \gamma_c) = \gamma_{\text{Voigt}}. \quad (24)$$

We note in passing that the expression for “ γ_{bulk} ” used for comparison with polycrystalline data in Ref. 28 is equal to $3\gamma_{\text{Voigt}}$.

Figure 9 shows values of $\gamma_{\text{Reuss}}(T)$ and $\gamma_{\text{Voigt}}(T)$ for BT and VFF4, together with estimated experimental values of

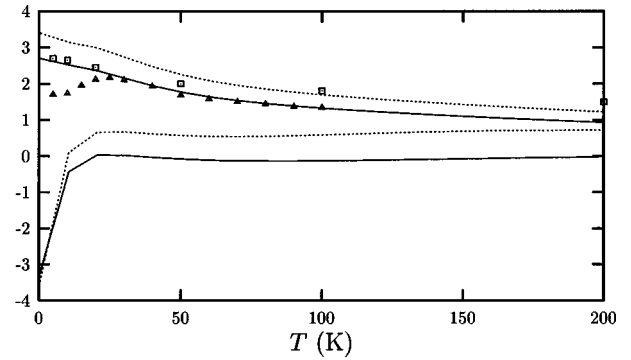


FIG. 9. The variation of the polycrystalline average γ_{Reuss} (two upper lines) and γ_{Voigt} (two lower lines) with temperature. ···, BT; —, VFF4. Experimental values of γ_{poly} , extrapolated to 100% crystallinity, are from Refs. 10 (Δ) and 12 (\square).

γ_{poly} from Refs. 10 and 12. VFF1 and VFF2 give values for γ_{Reuss} close to BT and VFF4, respectively. Since χ_a and χ_b are much larger than χ_c , γ_{Reuss} is dominated by γ_a and γ_b , whereas γ_{Voigt} is influenced equally by γ_c . The actual polycrystalline value will lie somewhere between these two limits, depending upon morphology. Our results agree with Gibbons’s conclusion³² that γ_{Reuss} is a closer estimate than γ_{Voigt} . At low temperatures Refs. 10 and 12 give similar results for α_{poly} , and so the disagreement between them for γ_{poly} must be due to their choice and processing of other data. We have also compared α_{poly} directly with α_{Reuss} and α_{Voigt} . Above about 50 K it is slightly below α_{Reuss} for VFF2 and VFF4; but at the lowest temperatures it falls well below γ_{Reuss} , though still well above γ_{Voigt} . This is at least partly because these models overestimate the low temperature expansion (see Sec. V E).

The rotational tension effect is negligible in γ_{Reuss} at all temperatures, but the nonrotational effect is important; e.g., in VFF2 it contributes negatively about 45% of the total at very low temperatures, falling to 35% above 100 K.

VI. FINAL REMARKS

We have shown how a simple atomistic model of polyethylene can throw light on the mechanisms of such complex processes as the anisotropic thermal expansion. Various sets of potential parameters, obtained in different ways, lead to the following conclusions.

Tensions caused by vibrations with components away from the interaction directions are responsible for the negative expansion along the polymer chains, and contribute significantly to the expansion perpendicular to the chains. Associated torques are unimportant, except at low temperatures where they have a marked effect on the anisotropy of expansion in the ab -plane. This anisotropy results from a subtle interplay of thermal stress and elasticity and is highly model dependent; it is only slightly affected by the decrease of setting angle with temperature and by other internal adjustments within the unit cell. Fine integration grids near the zone center give precise results at low temperatures, and demonstrate the importance of testing models against the available experimental data in this region; it is also predicted that the anisotropy in the ab plane at low temperatures will be much smaller than that measured by x-ray diffraction at

higher temperatures. T^3 behavior is approached closely only below 1 K.

This paper completes earlier work³⁻⁵ investigating mechanisms of thermal expansion in simplified models of polymer crystals. The methods will now be applied to more realistic models of specific materials, with the aim of understanding of how their macroscopic thermodynamic properties are related to crystal structure and bonding. This work will include applications to other polymeric systems, including those where long-range forces are relevant and where there are more atoms in the unit cell; and also to other complex crystals, such as those possessing layered structures. A full quasiharmonic treatment will be used, so taking account of the softening of crystal elasticity with increasing tempera-

ture. This will be carried out using both the direct minimization of the Helmholtz free energy with respect to external and internal degrees of freedom,¹⁸ and the analytic methods for deriving crystal properties and investigating mechanisms used in the present work.

ACKNOWLEDGMENTS

We thank the Royal Society and CONICET for support for a Joint Research Project with the University of Buenos Aires, and the Leverhulme Trust for support for J.A.O.B. The work was also supported by EPSRC Grant Nos. GR/K05979 and GR/L31340.

*Permanent address: Grupo de Química Teórica, Dpto. Química Inorgánica, Analítica y Química Física, Facultad de Ciencias Exactas y Naturales, Universidad de Buenos Aires. Pabellón 2, Ciudad Universitaria, (1428) Capital Federal, Argentina.

¹T. H. K. Barron, in *Thermal Expansion of Solids*, CINDAS Data Series on Material Properties, edited by C. Y. Ho (ASM International, Materials Park, OH, 1998), Vol. I-4, Chap. 1.

²T. H. K. Barron, T. G. Gibbons, and R. W. Munn, *J. Phys. C* **4**, 2805 (1971).

³R. M. Barron, T. H. K. Barron, P. M. Mummery, and M. Sharkey, *Can. J. Chem.* **66**, 718 (1988).

⁴K. R. Rogers, B. Sc. thesis, School of Chemistry, University of Bristol, 1988.

⁵T. H. K. Barron and K. J. Rogers, *Mol. Simul.* **4**, 27 (1989).

⁶H. Tadokoro, *Structure of Crystalline Polymers* (Krieger, Malabar, 1990).

⁷G. Avitabile, R. Napolitano, B. Pirozzi, K. D. Rouse, H. W. Thomas, and B. T. M. Willis, *J. Polym. Sci., Polym. Phys. Ed.* **13**, 351 (1975).

⁸G. T. Davis, R. K. Eby, and J. P. Colson, *J. Appl. Phys.* **41**, 4316 (1970).

⁹G. Dadobaev and A. I. Slutsker, *Sov. Phys. Solid State* **23**, 1131 (1981).

¹⁰I. Engeln, M. Meißner, and H. E. Pape, *Polymer* **26**, 364 (1985).

¹¹C. L. Choy, S. P. Wong, and K. Young, *J. Polym. Sci., Polym. Phys. Ed.* **22**, 979 (1984).

¹²G. K. White and C. L. Choy, *J. Polym. Sci., Polym. Phys. Ed.* **22**, 835 (1984).

¹³R. E. Taylor, in *Thermal Expansion of Solids* (Ref. 1).

¹⁴A. A. Maradudin, E. W. Montroll, G. H. Weiss, and I. P. Ipatova, *Theory of Lattice Dynamics in the Harmonic Approximation*, 2nd ed. (Academic, New York, 1971), Suppl. 3.

¹⁵T. H. K. Barron and M. I. Klein, in *Dynamical Properties of Solids*, edited by G. K. Horton and A. A. Maradudin (North-Holland, Amsterdam, 1974), Chap. 7.

¹⁶This is not recommended for quantitative calculations at higher temperatures. It has been found in practice that for many crystals a full application of the quasiharmonic approximation, including the variation of structure with temperature, extends its effective range to higher temperatures. See, e.g., G. D. Barrera, M. B. Taylor, N. L. Allan, T. H. K. Barron, L. N. Kantorovich, and W. C. Mackrodt, *J. Chem. Phys.* **107**, 4337 (1997).

¹⁷R. W. Munn, *J. Phys. C* **5**, 535 (1972).

¹⁸M. B. Taylor, G. D. Barrera, N. L. Allan, and T. H. K. Barron, *Phys. Rev. B* **56**, 14 380 (1997).

¹⁹T. H. K. Barron and A. Pasternak, *J. Phys. C* **20**, 215 (1987).

²⁰H. J. Monkhorst and J. D. Pack, *Phys. Rev. B* **13**, 5188 (1976).

²¹T. H. K. Barron, N. L. Allan, and J. A. O. Bruno (unpublished).

²²T. H. K. Barron and T. G. Gibbons, *J. Phys. C* **7**, 3260 (1974).

²³K. Tashiro, S. Minami, G. Wu, and M. Kobayashi, *J. Polym. Sci., Part B: Polym. Phys.* **30**, 1143 (1992).

²⁴M. Kobayashi and H. Tadokoro, *J. Chem. Phys.* **66**, 1258 (1977).

²⁵M. J. Hwang, T. P. Stockfisch, and A. T. Hagler, *J. Am. Chem. Soc.* **116**, 2515 (1994).

²⁶J. D. Gale, *J. Chem. Soc., Faraday Trans.* **93**, 629 (1997).

²⁷N. Karasawa, S. Dasgupta, and W. A. Goddard III, *J. Phys. Chem.* **95**, 2260 (1991).

²⁸D. J. Lacks and G. C. Rutledge, *J. Phys. Chem.* **98**, 1222 (1994).

²⁹K. Brugger and T. C. Fritz, *Phys. Rev.* **157**, 524 (1967).

³⁰K. Tashiro, M. Kobayashi, and H. Tadokoro, *Macromolecules* **11**, 914 (1978).

³¹J. F. Twisleton, J. W. White, and P. A. Reynolds, *Polymer* **23**, 578 (1982).

³²T. G. Gibbons, *J. Chem. Phys.* **60**, 1094 (1974).